



## Modeling laser-induced deformation patterns: Nonlinear effects and numerical analysis

D. WALGRAEF<sup>a,\*</sup> and N.M. GHONIEM<sup>b</sup>

<sup>a</sup>*Center of Nonlinear Phenomena and Complex Systems, Free University of Brussels, CP 231, Boulevard du Triomphe, B-1050 Brussels, Belgium*

<sup>b</sup>*Mechanical and Aerospace Engineering Department, The University of California at Los Angeles, Los Angeles, CA 90024, U.S.A.*

Received 20 July 1999; Accepted 1 October 1999

**Abstract.** The formation of laser-induced deformation patterns on thin films and surfaces may be described by a dynamical model for the coupled evolution of defect densities and deformation fields of the material. Increasing laser intensity induces deformational instability, which may be characterized in the framework of linear stability analysis of undeformed states. However, the selection and stability of deformation patterns are determined by nonlinear effects, and require full nonlinear analysis in the post-bifurcation regime. Analytical and numerical results are presented for uniform laser irradiation of pure metallic thin films, and the conditions for pattern selection are discussed.

**Keywords:** Defect microstructure, Deformation, Instability, Laser irradiation, Pattern formation, Thin film elasticity

### 1. Introduction

Laser-induced instabilities are becoming particularly important in several aspects of surface modification technologies. On the one hand, laser–surface interaction may control the structure and properties of thin films, coatings, semi-conductor surfaces. On the other hand, strong laser radiation induces structural and morphological changes in matter which are responsible for the degradation of light emitting devices, cumulative laser damage of optical components, non-uniform melting of semiconductor surfaces, to cite only a few of these aspects [1–4]. Furthermore, laser annealing and fast recrystallization may lead to special types of structures including molten and crystalline phases, and laser-assisted thin film deposition processes should also be in the mainstream of this activity [5]. Many of these phenomena proceed through the formation of regular structures on the surface of the material, and laser–surface interaction is evidently a field where patterning phenomena are overwhelming. Such deformation patterns are obviously the result of dynamical instabilities, and the methods of non-linear dynamics should thus allow us to describe and understand the mechanisms of pattern formation, selection and stability in films and coatings under laser irradiation.

The main instability mechanism in laser-irradiated materials is due to the coupling between defect dynamics and surface deformation [6]. The interaction of electromagnetic laser radiation with thin films leads to very strong absorption of photon energy in a shallow layer that is a few wavelengths deep from the surface. As a result, substantial non-equilibrium

---

\*Director of Research at the Belgian National Fund for Scientific Research. To whom correspondence should be addressed. E-mail: dwaelgr@ulb.ac.be

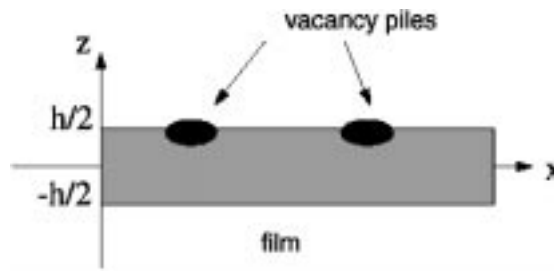


Figure 1. Geometrical set-up of a thin film under laser irradiation.

concentration of lattice defects is generated. The type of lattice defects depends on photon energy, wavelength of laser radiation and materials parameters. Examples of such defects are: electron-hole pairs in strongly absorbing semi-conductors, interstitials and vacancies in thin films, and voids and dislocation loops in prolonged irradiation. It is the coupling between defect generation, diffusion and the deformation field which leads to pattern-forming instabilities. As a result, the dynamical description of such phenomena should be based on the dynamics of the defect field  $N_d$  in the thin film and the elastic continuum of the host material described by the displacement vector  $\mathbf{U}(\mathbf{r}, t) = (U_x, U_y, U_z)$  with appropriate boundary conditions, both dynamics being coupled through the defect-strain interaction. Various types of defect structures may be induced by such dynamical systems. For example, in the case of thin films under laser irradiation, regular deformation patterns may appear on the film surface when the laser intensity exceeds some threshold. In spatially extended irradiation zones, one- and two-dimensional gratings have been widely observed [7,8]. In particular, when irradiation proceeds with focused beams, such as in laser-induced film deposition [6] or in etching experiments [9], rose-like deformation patterns are observed, where a finite number of petals develops around a central uniform spot. One striking experimental observation is that the number of petals increases with the intensity of the laser beam.

The system to be considered in this case is a thin film on a substrate, which is modeled by a thin horizontal crystalline layer submitted to a transverse laser beam. The geometry of the corresponding set-up is represented in Fig. 1.

Due to thermal heating induced by laser irradiation, an increased vacancy density is created in the subsurface layer. The corresponding transverse vacancy density profile results in a force on the film which may induce bending deformation. Even under uniform irradiation, this system may become unstable versus non-uniform deformations or vacancy density variations. Physically, a local increase in the vacancy density generates a lattice contraction in the film. This contraction has two effects: it locally reduces the defect formation energy, and, furthermore, induces a converging defect flux. As a result, both film contraction and local defect density will increase. On the other hand, a deformation bump in the film locally decreases the defect density. It furthermore increases the defect formation energy and induces an outgoing defect flux. In this case, a deformation bump will increase while the defect density will decrease. There is thus a feedback loop between local deformation and defect density variations, which provides a destabilizing mechanism for uniform deformations. However, vacancy diffusion tends to wash out non-uniformities in the system and provides a stabilizing mechanism for uniform defect densities. Instability occurs when the feedback loop effects dominate over diffusion, and this instability is of the Generation–Diffusion–Deformation–Instability type [6].

Two non-linear mechanisms saturate the growth of this instability. The first one comes from finite deformation elasticity, which limits the growth of the deformation. The second one results from vacancy dynamics, where the extra defect flux induced by surface deformation is proportional to the vacancy density. Consequently, defect fluxes from regions of decreasing defect density decrease accordingly in a feedback process which thus limits defect localization.

Hence, the dynamical model which can describe the evolution of such a system should be based on (i) a non-uniform transverse temperature field across the film, induced by laser irradiation; (ii) the evolution of vacancy density in strained crystals, including generation and transport; and (iii) the deformation of a thin film in the presence of a non-uniform vacancy density.

These three aspects have been analyzed elsewhere, and assembled in a full dynamical model, able to describe the main aspects of deformation patterning under laser irradiation [17,18]. Although pattern formation under extended and focused irradiation have already been described elsewhere, in the framework of this model [17–19], we will describe here, in more detail, how nonlinear effects determine stable patterns and their geometry. In particular, we will show that the geometry of selected patterns changes if the dominant nonlinear effects come from defect or elasticity fields. Furthermore, we will show that numerical analysis of the full dynamical model validates analytical results of the weakly nonlinear analysis, performed close to instability. The dynamical model and instability conditions for undeformed states are briefly recalled in Sections 2 and 3. Pattern selection is discussed in Section 4, where the role of nonlinear couplings between unstable modes is emphasized. Numerical confirmations of results obtained in Section 4 are presented in Section 5. Finally, conclusions are drawn in Section 5.1.

## 2. The dynamical model

The film is assumed to have a thickness  $h$ , and its dimensions in the  $x$  and  $y$  directions are assumed to be much larger than  $h$ . Its dynamics is supposed to be governed by the following coupled evolution of vacancy density,  $C$ , and transverse mid-plane film displacement,  $\xi$  [6,17]:

$$\begin{aligned} \partial_t C = & D_{\perp} \partial_{zz}^2 C + D_{\parallel} \Delta C - \frac{C}{\tau} + \vec{\nabla} \frac{\theta_v D_{\parallel} C}{kT} \vec{\nabla} (\vec{\nabla} \cdot \mathbf{U}) \\ & + \nabla_z \frac{\theta_v D_{\perp} C}{kT} \nabla_z (\vec{\nabla} \cdot \mathbf{U}) + g \exp\left[-\frac{E_f}{kT}\right] (1 + \theta_v \vec{\nabla} \cdot \mathbf{U}), \end{aligned} \quad (1)$$

where the first term on the right is the transverse vacancy diffusion rate, the second is the in-plane diffusion rate, the third is the rate of vacancy absorption on microstructural sinks, the fourth is the in-plane drift rate of vacancy transport due to displacement gradients in the film, the fifth is the transverse component of vacancy transport in the presence of the elastic field, and the sixth term is the vacancy generation rate in the presence of displacement gradients. Under usual experimental conditions,  $D_{\parallel} \tau \simeq 10^{-5} \text{ cm}^2$  and  $|\theta_v| \simeq 10^{-10} \text{ erg}$ .

$$\vec{\nabla} \cdot \mathbf{U} = -zm \Delta \xi, \quad (2)$$

$$\partial_t^2 \xi + \frac{c^2 h^2}{12} \Delta^2 \xi - \frac{c^2}{2} \sigma_{ij} \partial_{ij}^2 \xi + \frac{\theta_v}{\rho h} (C_+ - C_-) = 0, \quad (3)$$

where  $C_{\pm} = C(\vec{r}, \pm h/2, t)$  and

$$\sigma_{xx} \simeq ((\partial_x \xi)^2 + \nu(\partial_y \xi)^2) \quad (4)$$

$$\sigma_{yy} \simeq ((\partial_y \xi)^2 + \nu(\partial_x \xi)^2) \quad (5)$$

$$\sigma_{xy} \simeq -2(1 - \nu)(\partial_x \xi)(\partial_y \xi) \quad (6)$$

All kinetic coefficients and parameters are defined in Reference 17.

### 3. Instability of undeformed states

Let us consider the ideal situation of horizontally uniform irradiation of the film surface, which may adequately represent the case of thin films irradiated over large area by  $cw$  or pulsed lasers. We will furthermore assume that the temperature profile has reached its equilibrium value, or that its evolution is sufficiently slow, versus vacancy generation, to consider it as quasi-stationary. In the absence of deformation, the equilibrium vacancy density profile  $C^0(z)$  is then the solution of the steady state equation

$$\partial_t C^0 = D_{\perp} \partial_z^2 C^0 - \frac{1}{\tau} C^0 + g \exp\left[-\frac{E_f}{kT(z)}\right], \quad (7)$$

with the boundary conditions:

$$\partial_z C^0|_{z=h/2} = \partial_z C^0|_{z=-h/2} = 0. \quad (8)$$

Hence, the transverse variation of the defect density follows the temperature variation across the film. This profile is linear in the limit of a strong absorbing layer, and we may write:

$$T = T_+ + \frac{T_+ - T_-}{h} \left(z - \frac{h}{2}\right) \quad (9)$$

where  $T_+$  and  $T_-$  are the temperatures of upper and lower surfaces, respectively, and  $C^0(z)$  behaves as:

$$C^0(z) \simeq C_+^0 \exp \gamma \left(z - \frac{h}{2}\right), \quad (10)$$

where  $C_+^0 = g\tau \exp\left[-\frac{E_f}{kT_+}\right]$ , when  $\gamma \sqrt{D_{\perp} \tau} \ll 1$ , with  $\gamma = E_f \Delta T / kT_{\zeta}^2 h$ . This gives

$$C^0(h/2) = C_+^0, \quad C^0(-h/2) = C_+^0 e^{-\gamma h} = C_-^0. \quad (11)$$

The stability of the undeformed reference state versus spatial perturbations in the horizontal plane may be performed on studying the linear evolution of small perturbations of the undeformed state. Such perturbations are defined as  $n(\vec{r}, z, t) = C(\vec{r}, z, t) - C^0(z)$ , or, in particular,  $n_+(\vec{r}, t) = C_+ - C_+^0$  and  $n_-(\vec{r}, t) = C_- - C_+^0 \exp -\gamma h$ .

On performing the following scalings:

$$\begin{aligned} \partial_T &= \tau \partial_t, \quad \bar{\Delta} = \tau D_{\parallel} \Delta, \quad \mu = \frac{6m\theta_v^2 D_{\parallel} \tau}{\rho c^2 h^2 k}, \quad \beta = \frac{ch}{\sqrt{12} D_{\parallel}}, \quad \zeta = -\frac{h\theta_v}{2k D_{\parallel} \tau} \xi \\ N &= \mu(n_+ + n_-), \quad n = \mu(n_+ - n_-) \\ \epsilon &= \mu\left(\frac{C_+}{T_+} + \frac{C_-}{T_-}\right), \quad \eta = \mu\left(\frac{C_+}{T_+} - \frac{C_-}{T_-}\right) \end{aligned} \quad (12)$$

the dynamical model becomes:

$$\partial_T N = \Delta N - N - \eta \Delta(\Delta + 1)\zeta - \vec{\nabla}(\chi n + \delta N)\vec{\nabla}\Delta\zeta \quad (13)$$

$$\partial_T n = \Delta n - n - \epsilon \Delta(\Delta + 1)\zeta - \vec{\nabla}(\chi N + \delta n)\vec{\nabla}\Delta\zeta \quad (14)$$

$$\frac{1}{\beta^2} \partial_T^2 \zeta = -\Delta^2 \zeta - n + u \sigma_{ij}(\zeta) \partial_{ij}^2 \zeta, \quad (15)$$

where  $u = 6(2kTD_{\parallel}\tau/|\theta_v|h^2v)^2$ ,  $\chi = T_+ + T_-/2T_+T_-$  and  $\delta = T_+ - T_-/2T_+T_-$ .

The linear evolution matrix of the coupled deformation-defect system is then, in Fourier transform:

$$\begin{pmatrix} \frac{1}{\beta^2}\omega^2 + \bar{q}^4 & 1 & 0 \\ \epsilon\bar{q}^2(\bar{q}^2 - 1) & \omega + 1 + \bar{q}^2 & 0 \\ \delta\bar{q}^2(\bar{q}^2 - 1) & 0 & \omega + 1 + \bar{q}^2 \end{pmatrix}, \quad (16)$$

where  $\bar{q}$  is the dimensionless wave vector and the corresponding characteristic equation writes:

$$(\omega + 1 + \bar{q}^2) \left[ \left( \frac{1}{\beta^2} \omega^2 + \bar{q}^4 \right) (\omega + 1 + \bar{q}^2) - \epsilon \bar{q}^2 (\bar{q}^2 - 1) \right] = 0. \quad (17)$$

Since in realistic experimental conditions,  $c \simeq 10^5 \text{ cm.s}^{-1}$ ,  $h \simeq 10^{-2} \text{ cm}$ , and  $D_{\parallel} \simeq 10^{-5} \text{ cm}^2.\text{s}^{-1}$ , one has  $\beta \gg 1$ , and the relevant root for instability is:

$$\omega_1 = \epsilon \left( 1 - \frac{1}{\bar{q}^2} \right) - (1 + \bar{q}^2). \quad (18)$$

Hence,  $\epsilon$  plays the role of a bifurcation parameter, and the instability threshold is given by the minimum of the marginal stability curve

$$\epsilon = \frac{\bar{q}^2(\bar{q}^2 + 1)}{\bar{q}^2 - 1}. \quad (19)$$

or

$$\epsilon_c = (1 + \sqrt{2})^2 \simeq 5.8, \quad q_c^4 = \epsilon_c \quad (20)$$

where  $q$  is the scaled wavenumber.

Above the instability threshold, there is a band of unstable wave vectors, going from  $q_m$  to  $q_M$ , where

$$q_{M(m)}^2 = \frac{1}{2} [\epsilon - 1 \pm \sqrt{(B - 1)^2 - 4\epsilon}] \quad (21)$$

The modes with maximum growth rate correspond to dimensionless wavenumber  $q_0 = \epsilon^{1/4}$ , or to unscaled wavelength

$$\lambda_0 = 2\pi \sqrt{\tau D_{\parallel}} \epsilon^{-1/4} = 2\pi l \epsilon^{-1/4} \quad (22)$$

Hence, it may be expected that spatial modulations of wavenumber  $q$  equal to or close to  $q_0$  will grow first, leading to the formation of a deformation pattern with a wavelength which is typically of the order of  $10 \mu\text{m}$  [17]. It is interesting to note that Equation 22 provides a simple physical interpretation of the selected pattern wavelength. The main dependence is on

the vacancy mean-free path, with weak contributions from the critical bifurcation parameter. Thus, the wavelength  $\lambda_0$  is of the order of 10 times the vacancy mean-free path in most systems. In a well-annealed thin film,  $\lambda_0 \simeq 10 \mu\text{m}$ , with  $l \simeq 1 \mu\text{m}$ , consistent with experimental observations [7,8]. However, if other experimental conditions correspond to a thin film that contains a high density of initial defects, the vacancy mean-free path would be short, and the corresponding pattern wavelength small. This finding can be readily tested in appropriate experimental settings.

In isotropic systems, there is an orientational degeneracy in the problem, since the instability threshold and the linear growth rate of the unstable modes only depend on  $q^2$ . Under these conditions, not only all the modes of the unstable band may grow, but also unstable modes with any orientation may equally grow. The survivors, and of course the final selected patterns are determined by their nonlinear interactions. Thus, nonlinear saturation terms of the dynamics will determine which structure should be selected and what its stability domain should be. This study evidently requires a nonlinear analysis beyond instability, which will be discussed now.

#### 4. Weakly nonlinear analysis and pattern selection

In the weakly non-linear regime beyond a pattern-forming instability, the dynamics may be reduced to the evolution of an order parameter-like variable which corresponds to the unstable modes [13]. In the present case, this reduction may be performed in the framework of the adiabatic elimination of the stable modes [12]. In the case of uniform (or extended) irradiation, one is the total mean defect density,  $N$ , which is the eigenmode corresponding to the eigenvalue  $\omega(4) = -(1 + q^2)$  of the linear evolution matrix. The second one is the transverse displacement of the mid-plane,  $\zeta$ , that may also be adiabatically eliminated since the characteristic time scale of its evolution,  $\beta$ , is negligibly small. These two variables may thus be expressed, in Fourier transform, as a series expansion in powers of  $n$ . This expansion, deduced from the dynamical system (Equations 13–15), gives, up to the first relevant contributions [17]:

$$\begin{aligned} \tau_0 \partial_T n_{\vec{q}} &= [\bar{\epsilon} - \Lambda(q^2 - q_c^2)^2] n_{\vec{q}} + v \int_c d\vec{k} (\vec{1}_q \cdot \vec{1}_k) n_{\vec{q}-\vec{k}} n_{\vec{k}} \\ &\quad - \int_c d\vec{k} \int_c d\vec{k}' g(\{\vec{1}_q\}) n_{\vec{q}-\vec{k}-\vec{k}'} n_{\vec{k}} n_{\vec{k}'} + \dots \end{aligned} \quad (23)$$

where  $\tau_0 = 2 + \sqrt{2}$ ,  $\bar{\epsilon} = (\epsilon - \epsilon_c)/\epsilon_c$  and  $q^2 - q_0^2/q_0^2$ ,  $\Lambda = \tau_0/q_0^2$ ,  $v = \tau_0(\delta + \chi\eta/\epsilon_c)$  and  $g = (u/q_0^8) \sum_{i,j} E_{ij}(\{\vec{1}_q\}) + \tau_0 \chi(\chi + \delta\eta/\epsilon_c) \cdot (\vec{1}_q \cdot \vec{1}_k) ((\vec{1}_q - \vec{1}_k) \cdot \vec{1}_{k'}) (1/1 + 2q_0^2(1 - (\vec{1}_q \cdot \vec{1}_k)))$ .  $n_{\vec{q}}$  is the order parameter-like variable, and, in the weakly non-linear regime around the instability, the expansion may be limited to cubic nonlinearities, which are the first relevant contributions for the saturation of the instability. One may now discuss pattern selection and stability through the analysis of the corresponding amplitude equations, which may be easily obtained from Equation 23.

The simplest pattern one may think of corresponds to stripes, which are defined, in real space, by  $n = A e^{iq_0 x} + \bar{A} e^{-iq_0 x}$  (the choice of the wave-vector orientation is arbitrary, as a result of the isotropy of the model, and the following results do not depend on it). The asymptotic evolution of their amplitudes is then given, at the lower order in  $\bar{\epsilon}$ , by [12]:

$$\tau_0 \partial_T A = \bar{\epsilon} A + \zeta_0^2 \partial_x^2 A - g A |A|^2 \quad (24)$$

where  $\zeta_0^2 = 4q_c^2\Lambda$ , and  $g = u\epsilon_c/q_0^8 + 2/(1 + 4q_0^2)$ .

This equation admits the following family of steady-state solutions:

$$A_0 = \sqrt{\bar{\epsilon} - \zeta_0^2 k^2} e^{i(kx + \Phi)}, \quad (25)$$

$\Phi$  being an arbitrary phase variable. These solutions are stable versus long wavelength perturbations in the range  $0 \leq k \leq \sqrt{\bar{\epsilon}/3\zeta_0^2}$  (zig-zag and Eckhaus stability limits [14]). Furthermore, the stripes with maximum growth rate are the critical ones ( $k = 0$ ).

Due to the structure of the evolution Equation 23, one has to test the stability of the critical stripe solutions Equation 25 versus modulations with wave vectors making an arbitrary angle  $\phi$  with its own wave-vector direction (say e.g.  $x$ ), and of amplitude  $A_\phi$ . For  $\phi \neq 2\pi/3$ , there is no contribution in their dynamics that comes from the quadratic term of Equation 23, and their linear growth rate, in the presence of the stripes Equation 25, is then:

$$\tau_0 \partial_T A_\phi = \bar{\epsilon}(1 - \gamma(\phi))A_\phi + \zeta_0^2 (\vec{1}_\phi \cdot \vec{\nabla})^2 A_\phi \quad (26)$$

where

$$\gamma(\phi) = \frac{\frac{4 \cos^2(\phi)}{(1+2q_0^2)^2 - 4q_0^4 \cos^2(\phi)} + \frac{u\epsilon_c}{q_0^8} [2\nu + 2(1 - \nu)] \cos^2(\phi)}{\frac{2}{1+4q_0^2} + \frac{u\epsilon_c}{q_0^8}} \quad (27)$$

The first part of this term dominates when the non-linearities arising from the bending equation are negligible versus the non-linearities of the defect dynamics (this corresponds to  $u \ll 1$  or film thickness  $h \geq 5 \mu\text{m}$  typical experimental conditions), while the second part, which is of the Proctor–Sivashinsky type of coupling [15,16], dominates when non-linearities of the defect dynamics become negligible, which is the case for thinner films, such that  $u \gg 1$  (or  $h \leq 5 \mu\text{m}$  for typical experimental conditions). The maximum growth rate for these modulations corresponds to the minimum of  $\gamma(\phi)$ , and, for Poisson ratios in the physically acceptable range ( $0 \leq \nu \leq 1/2$ ),  $\gamma(\phi)$  is minimum for  $\phi = \pi/2$ , where it is always less than one. The result of this analysis is that stripes are always unstable, in isotropic systems, versus rectangular bimodal patterns.

The amplitude equations of such patterns, defined as  $n = A \exp i q_0 x + B \exp i q_0 y + c.c.$  are:

$$\begin{aligned} \tau_0 \partial_T A &= \bar{\epsilon} A + \zeta_0^2 \partial_x^2 A - g A (|A|^2 + \gamma(\frac{\pi}{2}) |B|^2) \\ \tau_0 \partial_T B &= \bar{\epsilon} B + \zeta_0^2 \partial_x^2 B - g B (|B|^2 + \gamma(\frac{\pi}{2}) |A|^2) \end{aligned} \quad (28)$$

and the uniform steady-state solution corresponds to:

$$|A|^2 = |B|^2 = \frac{\bar{\epsilon}}{g} \frac{2q_0^8 + \epsilon_c u (1 + 4q_0^2)}{2q_0^8 + \epsilon_c u (1 + 2\nu)(1 + 4q_0^2)} \quad (29)$$

When quadratic terms are irrelevant ( $\nu \simeq 0$ ), which is the case when temperature and defect densities are nearly uniform across the film thickness, square planforms are stable when elastic nonlinearities dominate, i.e. when the film is sufficiently thin to behave as a membrane. However, when the film is thicker, and behaves as a plate, defect nonlinearities dominate, and  $\gamma(\phi) \simeq 2 \cos^2 \phi / (1 + a \sin^2 \phi)$ , with  $a = 4q_0^4 / (1 + 4q_0^2)$  ( $a \simeq 2.3$  at  $\epsilon = \epsilon_c$ ).

In this case, it is easy to show that square planforms are unstable versus modulations with an angle in the range defined by  $\cos^2 \phi = (1 + a)/(2 + a)$ . As a result, square planforms are most unstable versus modulations with  $\phi = \frac{\pi}{4}$ , leading to multimodal patterns formed by four pairs of wave vectors separated by angles of  $\pi/4$ ,  $\pi/2$  and  $3\pi/4$ . The growth rate of  $\pi/4$  modulations ( $\frac{a}{1+a}$ ) is, however, smaller than the growth rate of supercritical hexagonal modulations from stripes  $\frac{1+3a}{2+3a}$ . Under these conditions, supercritical hexagonal patterns are expected to be dynamically selected (see Fig. 3). Note that supercritical hexagons may easily be recognized from subcritical ones. For subcritical hexagons, the sum of the phases of the underlying triplet of unstable modes is fixed, which is not the case for supercritical ones. As a result, in the first case, the maxima of the order parameter-like variable remain strictly on a hexagonal (or triangular) lattice throughout the system [12], while in the latter case, domains may develop, with different positions of the maxima on the lattice (cf. Fig. 3).

For increasing  $\bar{\epsilon}$ ,  $a$  increases, and the range of unstable angles becomes wider. Supercritical hexagonal planforms may, in turn, become unstable versus patterns built on  $n > 3$  pairs of modes, and that are of the quasi-crystalline type (see Fig. 4). Note that these quasiperiodic patterns appear here as a natural consequence of the form of the non-linear couplings as suggested in Reference 20, and do not require particular combinations of external forcing as in other systems [21,22].

When quadratic nonlinearities are relevant, i.e. when  $v \neq 0$ , subcritical patterns may also develop in the system. They correspond to hexagonal planforms built on modulations with wave vectors making  $2\pi/3$  angles between them. In this case the order parameter-like variable writes as:

$$n = A_1 e^{i\vec{q}_1 \vec{r}} + A_2 e^{i\vec{q}_2 \vec{r}} + A_3 e^{i\vec{q}_3 \vec{r}} + c.c. \quad (30)$$

with  $\vec{q}_1 + \vec{q}_2 + \vec{q}_3 = 0$ ,  $|\vec{q}_i| = q_0$ , and the corresponding amplitude equations are [14]:

$$\begin{aligned} \tau_0 \partial_T A_1 &= [\bar{\epsilon} + \frac{\zeta_0^2}{4q_0^2} (\vec{q}_1 \vec{\nabla})^2] A_1 - \frac{v}{2} \bar{A}_2 \bar{A}_3 - g A_1 (|A_1|^2 + \gamma (\frac{2\pi}{3}) (|A_2|^2 + |A_3|^2)) \\ \tau_0 \partial_T A_2 &= [\bar{\epsilon} + \frac{\zeta_0^2}{4q_0^2} (\vec{q}_2 \vec{\nabla})^2] A_2 - \frac{v}{2} \bar{A}_1 \bar{A}_3 - g A_2 (|A_2|^2 + \gamma (\frac{2\pi}{3}) (|A_1|^2 + |A_3|^2)) \\ \tau_0 \partial_T A_3 &= [\bar{\epsilon} + \frac{\zeta_0^2}{4q_0^2} (\vec{q}_3 \vec{\nabla})^2] A_3 - \frac{v}{2} \bar{A}_1 \bar{A}_2 - g A_3 (|A_3|^2 + \gamma (\frac{2\pi}{3}) (|A_1|^2 + |A_2|^2)) \end{aligned} \quad (31)$$

Uniform solutions of amplitude

$$|A_1| = |A_2| = |A_3| = \frac{1}{4g(1 + 2\gamma(\frac{2\pi}{3}))} [v + \sqrt{v^2 + 16g\bar{\epsilon}(1 + 2\gamma(\frac{2\pi}{3}))}] \quad (32)$$

exist for these equations and are stable for [14]:

$$-\frac{v^2}{16g(1 + 2\gamma(\frac{2\pi}{3}))} \leq \bar{\epsilon} \leq \frac{3v^2}{16g(1 - \gamma(\frac{2\pi}{3}))^2} \quad (33)$$

if  $\gamma(2\pi/3) > 1$ . If  $\gamma(2\pi/3) \leq 1$ , which is the case here, they are stable in all the range  $-(v^2/16g(1 + 2\gamma(\frac{2\pi}{3}))) \leq \bar{\epsilon}$ .

Furthermore, linear stability analysis shows that squares are unstable versus hexagons for

$$0 \leq \bar{\epsilon} \leq \frac{v^2}{2g(\gamma(\frac{2\pi}{3}) + \gamma(\frac{\pi}{6}))} = \epsilon_h \quad (34)$$

On the other hand, families of hexagons with  $|\vec{q}_i| = q_0 + k \neq q_0$  may also be steady-state solutions of Equation 31. Their amplitude varies as Equation 32, with  $\bar{\epsilon} = \bar{\epsilon} - \zeta_0^2 k^2$ . Their phase stability may be studied along the usual procedure [12]. Since  $\gamma(\frac{2\pi}{3}) \leq 1$ , one then finds that such hexagons exist in the range  $\bar{\epsilon} > -((v^2)/(16g(1 + 2\gamma(\frac{2\pi}{3})))) + \zeta_0^2 k^2$ , and are phase stable in the range  $\bar{\epsilon} > -(v^2)/(64g(1 + 2\gamma(\frac{2\pi}{3}))) + 8\zeta_0^2 k^2 + O(k^3)$ .

In the case of membrane behavior of thin films, squares and hexagons may thus be simultaneously stable for  $\bar{\epsilon} > \epsilon_h$ . Hence, since squares are unstable at instability (for  $0 \leq \bar{\epsilon} \leq \epsilon_h$ ), hexagonal deformation patterns should always be observed for steady increase of laser intensity. For ‘quench’ experiments, i.e. when laser irradiation is initiated suddenly in the range  $\bar{\epsilon} > \epsilon_h$ , either squares or hexagons could be observed, as the result of their bistability.

## 5. Numerical analysis

From the point of view of pattern formation phenomena, the formation of supercritical quasi-periodic patterns, due to the particular form of the cubic nonlinearities of the order parameter-like equation (Equation 23) is original. To check the predictions of the weakly nonlinear analysis, the model (Equations 13–15) has been studied numerically, when  $\eta = \delta = 0$ , which rules out subcritical bifurcations, and thus mimics the behavior of uniform systems with negligible transverse temperature gradients. The method used is an explicit Euler method in Fourier space, with an iterative resolution of the nonlinear deformation equation for the bending coordinate. The system corresponds to  $128 \times 128$  or  $256 \times 256$  grids with periodic boundary conditions. The initial values of the variables were fixed at  $N = n = \zeta = 0$  with 1% noise on the  $n$ -variable. In the thin (‘membrane’) film regime ( $u \gg 1$ ), square patterns are obtained, in confirmation of the analytical results (see Fig. 2). In the ‘thick’ or ‘plate’ regime ( $u \ll 1$ ), supercritical hexagonal (see Fig. 3) and quasi-periodic patterns are obtained. By increasing the bifurcation parameter, it may effectively be shown that stable patterns with  $n = 3, 4, 5, 6$  and 8 pairs of wave vectors are successively produced. There is thus a basic agreement between the results of the amplitude equation description and the numerical analysis of the complete dynamical system, although quasi-periodic patterns were obtained for relatively high values of the bifurcation parameter. An example of such a pattern is presented in Fig. 4. In this figure, the upper left figure represents the spatial pattern in real space, while the upper right figure corresponds to the same pattern in Fourier space. The lower figure shows the intensity of the Fourier spectrum of the pattern versus wave vector. The Fourier spectrum is computed from the numerical solutions of the dynamical model. Besides the good definition of the pattern symmetry, one should note the sharp wavenumber selection.

### 5.1. CONCLUSIONS

A dynamical model describing the coupled evolution of defect and elasticity fields in thin films under intense laser irradiation has been shown to be able to predict the formation of deformation patterns on the film surface. Previous analysis has shown that the threshold for mechanical instability of laser-irradiated thin films is controlled by a bifurcation parameter  $\epsilon$ , which can be written as

$$\epsilon = \epsilon_1 \cdot \epsilon_2 \cdot \epsilon_3 \tag{35}$$

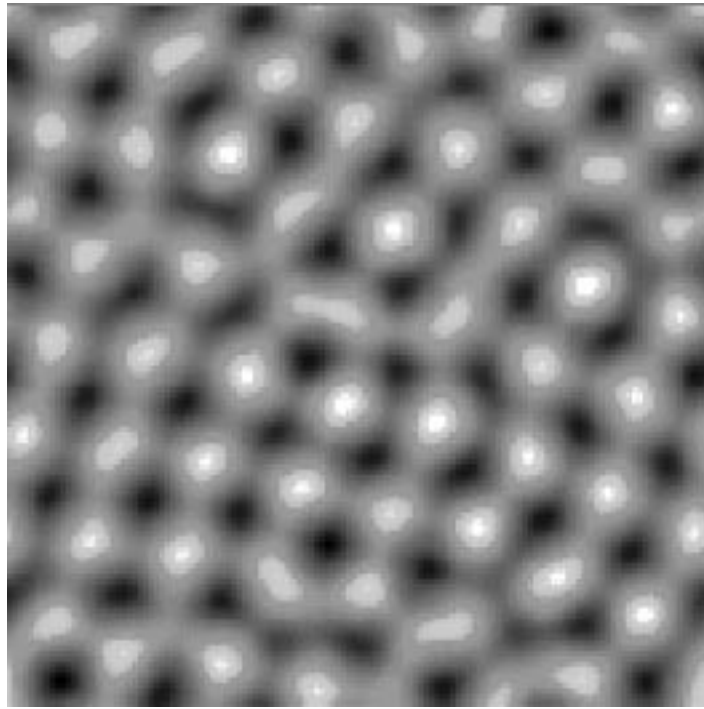


*Figure 2.* Square-like patterns obtained in the numerical analysis of the dynamical model for thin film behavior of the irradiated layer ( $u \rightarrow \infty$ ,  $\epsilon = 6.5$  or  $\bar{\epsilon} \simeq 0.1$ ).

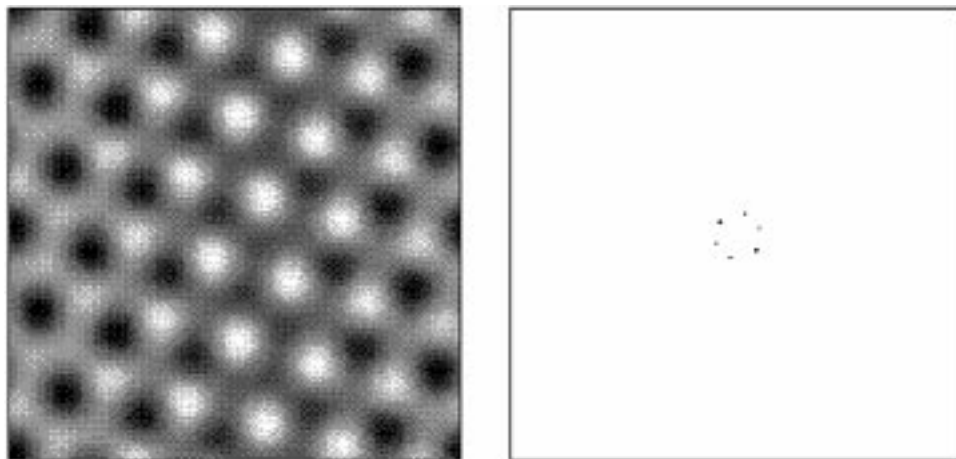


*Figure 3.* Supercritical hexagonal pattern, and its Fourier transform, obtained in the numerical analysis of the dynamical model for plate behavior of the irradiated layer ( $u \rightarrow 0$ ,  $\epsilon = 6$  or  $\bar{\epsilon} \simeq 0.03$ ).

where

$$\epsilon_1 = \frac{\bar{C}\theta_v}{\rho c^2} \tag{36}$$

and  $\bar{C}$  is a suitable mean vacancy concentration,

$$\epsilon_2 = \frac{\theta_v}{kT} \tag{37}$$

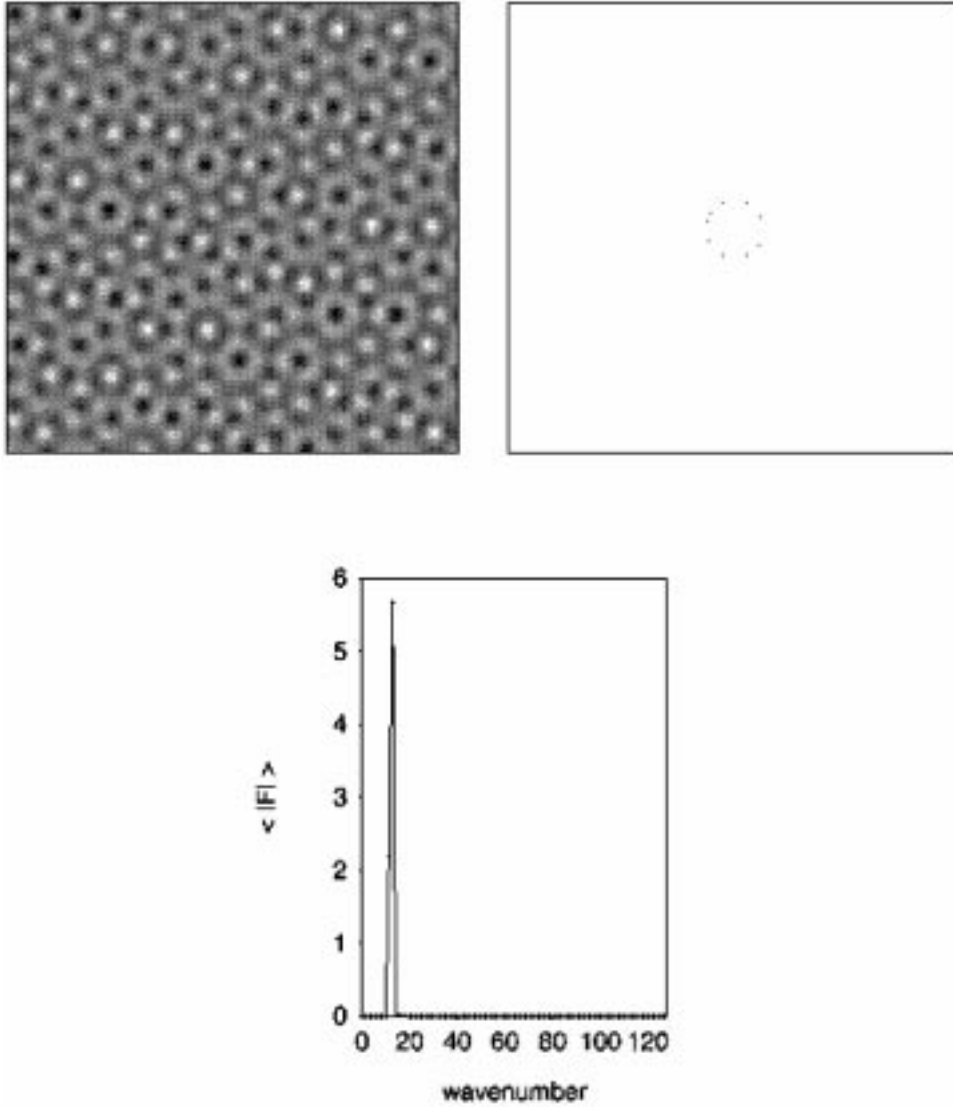


Figure 4. Patterns with fivefold symmetry obtained in the numerical analysis of the dynamical model for plate behavior of the irradiated layer ( $u \ll 1$ ,  $\epsilon = 34$  or  $\bar{\epsilon} \simeq 4.7$ ) (upper left: pattern, upper right: Fourier transform, down: spectrum versus wavenumber).

and  $\bar{T}$  is a suitable mean temperature,

$$\epsilon_3 = \frac{D_{\parallel} \tau}{h^2} = \left(\frac{l}{h}\right)^2 \quad (38)$$

where  $l$  is the mean-free path of a vacancy in the thin film.

The physical meaning of the components of the bifurcation parameter is as follows.  $\epsilon_1$  is a measure of the ratio of the energy stored in lattice defects to the kinetic energy associated with sound propagation in the film. The parameter  $\epsilon_2$  is a measure of the energy decrease of an atom near a vacancy to its thermal energy, and  $\epsilon_3$  is a measure of the ratio of the vacancy mean-free path to the film thickness.

The linear stability analysis derived from the present model is only adequate for studies related to the onset of thin film instability. However, for obvious practical purposes, it is essential to determine and predict the nature of selected patterns and their dependence on material and irradiation conditions. This can only be done by considering the influence of non-linear effects in the model.

Effectively, horizontally uniform vacancy distributions and film deformations are easily shown to become unstable above a threshold value of the bifurcation parameter, but the linear analysis only determines a preferred wavelength for the deformation patterns that are expected to form beyond the instability. However, pattern symmetry, selection and stability properties strongly depend on non-linear dynamical effects. For example, when the film is sufficiently thin, and behaves as a membrane, elastic nonlinearities dominate over defect nonlinearities, and selected patterns may correspond to square or hexagonal planforms. On the other hand, in thicker films, with small transverse temperature gradients, defect nonlinearities dominate over elastic ones, and quasi-periodic patterns should be observed in this regime.

In closing, we may thus list here the following significant conclusions from the above nonlinear analysis.

- (1) One-dimensional gratings are unstable in an isotropic system. Consistency with experimental observations may thus require anisotropies in the diffusion and elastic fields. In systems where the interaction between the laser field and the film surface depends on crystal symmetries, such gratings could appear, triggered by anisotropic couplings.
- (2) On increasing the bifurcation parameter in very thin films, square patterns and hexagonal ones become simultaneously stable.
- (3) Stable quasi-periodic patterns should be observed to occur in thin plates, with small transverse temperature gradients.
- (4) It is somewhat surprising to note that linear aspects of the instability (e.g. threshold and critical wavelength) do not depend on the exact shape of vacancy or temperature profiles across the film. Weakly adherent thin films appear to be unstable for any heating mechanism which generates sufficient concentration of vacancies. However, the geometry of the selected patterns is very sensitive to such profiles, through their influence on nonlinear dynamical effects.

### **Acknowledgements**

The contribution of Dr. J. Lauzeral to the numerical analysis is gratefully acknowledged. Financial support has been provided by a grant from the Belgian National Fund for Scientific Research.

### **References**

1. Kossowsky, R. and Singhal, S.C., *Surface Engineering, Surface Modification of Materials*, Martinus Nijhoff, Dordrecht, 1984.
2. Laude, L., Bauerle, D. and Wauthélet, M., *Interfaces under Laser Irradiation*, Martinus Nijhoff, Dordrecht, 1987.
3. Walgraef, D. and Ghoniem, N.M., *Patterns, Defects and Materials Instabilities*, Kluwer Academic Publishers, Dordrecht, 1990.
4. McConnell, R. and Noufi, R., *Science and Technology of Thin Film Superconductors*, Plenum, New York, NY, 1990.

5. Preston, J.S., Sipe, J.E. and van Driel, H.R., In Laude, L., Bauerle, D. and Wauthélet, M. (Eds.) *Interfaces under Laser Irradiation*, Martinus Nijhoff, Dordrecht, 1987, pp. 127–136.
6. Emel'yanov, V.I., *Laser Phys.*, 2 (1992) 389.
7. Banishev, A.F., Emel'yanov, V.I. and Novikov, M.M., *Laser Phys.*, 2 (1992) 192.
8. Young, J.F., Preston, J.S. and van Driel, H.R., *Phys. Rev.*, B27 (1983) 1141, 1155.
9. Mogyrosi, P., Piglmayer, K. and Bauerle, D., *Surface Sci.*, 208 (1989) 232.
10. Bauerle, D., *Laser Processing and Chemistry*, Springer Verlag, New York, NY, 1996.
11. Landau, L.D., *Theory of Elasticity*, Pergamon Press, Oxford, 1986.
12. Walgraef, D., *Spatio-Temporal Pattern Formation (with examples in physics, chemistry and materials science)*, Springer Verlag, New York, NY, 1996.
13. Cross, M.C. and Hohenberg, P.C., *Rev. Mod. Phys.*, 65 (1993) 851.
14. Borckmans, P., Dewel, G., De Wit, A. and Walgraef, D., In Kapral, R. and Showalter, K. (Eds.) *Chemical Waves and Patterns*, Kluwer, Dordrecht, 1994, pp. 323–363.
15. Proctor, M.R.E., *J. Fluid Mech.*, 113 (1981) 469.
16. Gertsberg, V.L. and Sivashinsky, G.I., *Prog. Theor. Phys.*, 66 (1981) 1219.
17. Walgraef, D., Ghoniem, N.M. and Lauzeral, J., *Phys. Rev.*, B56 (1997) 15361.
18. Lauzeral, J., Walgraef, D. and Ghoniem, N.M., *Phys. Rev. Lett.*, 79 (1997) 2706.
19. Walgraef, D., *J. Eng. Mater. Technol.*, 121 (1999) 182.
20. Walgraef, D., Borckmans, P. and Dewel, G., *Nature*, 318 (1985) 606.
21. Newell, A.C. and Pomeau, Y., *J. Phys.: Math. Gen.*, 26 (1993) L429.
22. Edwards, W. and Fauve, S., *Phys. Rev.*, E47 (1993) R788.